

Mesoscopic transport in electrostatically-defined spin-full channels in quantum Hall ferromagnets

Aleksandr Kazakov,¹ George Simion,¹ Yuli Lyanda-Geller,^{1,2} Valery Kolkovsky,³
Zbigniew Adamus,³ Grzegorz Karczewski,³ Tomasz Wojtowicz,^{4,3} and Leonid P. Rokhinson^{1,2,5,*}

¹*Department of Physics and Astronomy, Purdue University, West Lafayette, IN 47907 USA*

²*Birck Nanotechnology Center, Purdue University, West Lafayette, IN 47907 USA*

³*Institute of Physics, Polish Academy of Sciences, Al. Lotnikow 32/46, 02-668 Warsaw, Poland*

⁴*International Research Centre MagTop, al. Lotnikow 32/46, PL 02-668 Warszawa, Poland*

⁵*Department of Electrical and Computer Engineering,
Purdue University, West Lafayette, IN 47907 USA*

Development of a two-dimensional systems with reconfigurable one-dimensional topological superconductor channels became primary direction in experimental branch of Majorana physics. Such system would allow to probe non-Abelian properties of Majorana quasiparticles and realize the ultimate goal of Majorana research - topological qubit for topologically protected quantum computations. Here we propose and develop a new platform to support and manipulate non-Abelian excitations which is based on ferromagnetic transitions in a quantum Hall effect regime. Electrostatic control of ferromagnetic transition at $\nu = 2$ in high mobility 2D gases in CdMnTe allows formation of domain walls along gate boundary, and we show that short ($< 4 \mu\text{m}$) channels are conducting at low temperatures. We show that channels resistance is invariant under field inversion, unlike chiral channels formed between different QHE states. Coupled to a s-wave superconductor these channels should support Majorana excitations.

INTRODUCTION

Development of a reconfigurable network of one-dimensional p-wave superconductors is a prerequisite for the demonstration of topologically protected qubits [1, 2]. The majority of experimental and theoretical effort is devoted toward superconductor/semiconductor nanowire hybrids [3–9] or topological insulator (TI) 2D edges [10], where combination of spin-orbit interaction and magnetic field lifts fermion doubling while retaining both spin polarizations. Coupled to a conventional s-wave superconductor such one-dimensional systems mimics Kitaev's chain with Majorana fermions formed at the ends of the wire [1].

There is another completely overlooked class of objects where fermion doubling is lifted but both spin polarizations are preserved, namely domain walls (DW) formed during quantum Hall ferromagnetic (QHFm) transition, where DWs form a quasi one-dimensional helical channels [11, 12]. Unlike nanowires, where multi-channel transport can render induced superconductivity to be topologically trivial [3], single energy level transport in QHFm DWs is topologically protected by a cyclotron gap. QHFm transitions, where polarization of the top-most energy level changes polarization, have been observed in GaAs quantum wells with vanishing g-factor [13], in magnetic semiconductors [14], and for some fractional QHE states in GaAs [15], CdMnTe [16] and graphene [17]. DWs formed in a fractional QHE regime are of particular interest because they provide a path to form higher-order non-Abelian excitations [18], which are more suitable for topologically protected quantum computation [19].

QHFm transition results from a competition between cyclotron, Zeeman and exchange energies, and is conventionally investigated by varying in-plane (Zeeman) magnetic field. During QHFm transition a uniform 2D gas spontaneously phase-separate into insulating magnetic domains [20] and electrical current flows along a random network of DWs. In CdMnTe QW Landau level (LL) spin-splitting energy has two contributions [21]: a positive s-d exchange term $\chi x_{Mn} E_{sd}$ and a negative Zeeman term $g^* \mu_B B$, where χ is an overlap between electron wavefunction in a well and Mn, x_{Mn} is Mn concentration, $E_{sd} \approx 220$ meV, $g^* = -1.6$ for CdTe, μ_B is Bohr magneton, and we neglected B and T -dependence of exchange at low T and moderate B . Competition between these two terms leads to an unusual energy spectrum, Fig.1a, where Landau levels with opposite spins cross at some magnetic field B^* . Engineering placement of Mn within the quantum well allows electrostatic control of the s-d overlap $\chi = \chi(V_g)$ and, thus, a local control of QHFm transition [22] $B^*(V_g)$. At domains boundaries two counter-propagating edges with opposite polarization form DWs, as shown schematically in Fig.1b for the QHFm transition at a filling factor $\nu = 2$. Coupled to superconducting contacts these DWs should support Majorana fermions in the integer QHE regime and parafermions in the fractional QHE regime.

Past studies of QHFm were focused on the physics of a 2D phase transition [13, 14, 23] and did not investigate DWs *per se*. In this work we use electrostatic control of exchange interaction and QHFm transition to form conductive channels between domains with different polarization and to study electrical transport through channels of different length and width.

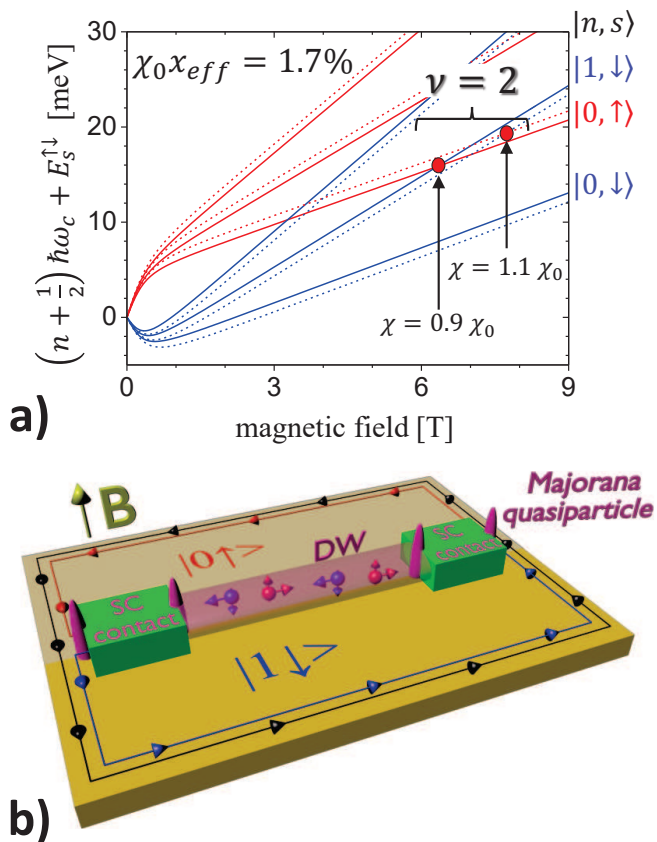


FIG. 1. (a) Fan diagrams of Landau levels for different s - d overlaps χ and effective Mn doping $\chi_0 x_{eff} = 1.7\%$. Ferro-magnetic phase transition for filling factor $\nu = 2$ are marked by red dots. (b) Formation of helical domain walls in a quantum Hall regime. Spin polarization of the top energy level is switched under a top gate (yellow) and a DW is formed along the gate boundary. With induced superconductivity from superconducting contacts (green) non-Abelian excitations (magenta) are expected to be formed at the boundaries between topological superconductivity induced in the helical DW and s -wave superconducting contacts.

SAMPLES

Devices were fabricated from CdMnTe/Cd_{0.8}Mg_{0.2}Te QW heterostructures grown by molecular beam epitaxy (MBE), see Refs. [14, 16] for details. QW is 30 nm wide and is modulation doped with iodine. Mn is introduced into the QW as 7 δ -doping layers spaced by 6 monolayers of CdTe starting 13 nm from the bottom of the quantum well in the growth direction. Effective Mn concentration is 1.5%–1.7% as determined from the position of QHFm transition B^* . We found B^* to depend on the cooldown conditions and LED illumination which most likely affects wavefunction profile within the quantum well and, thus, the overlap χ . Electrostatic control of $\chi(V_g)$ affords $\sim 10\%$ control of the exchange and B^* with both front (V_{fg}) and back (V_{bg}) gates, see Fig.2b. Low tem-

perature density and mobility are $3 - 3.5 \cdot 10^{11} \text{ cm}^{-2}$ and $3 - 4 \cdot 10^4 \text{ cm}^2/\text{V}\cdot\text{s}$ respectively.

Samples are patterned in a number of alternating gated and ungated Hall bar sections with typical sizes $\sim 20 - 30 \mu\text{m}$, see Fig.2a, with thin (10–15 nm) semi-transparent Ti layer serving as a front gate. Gated and ungated sections are separated by narrow constrictions of various widths with gate boundary aligned with the constriction (inset in the Fig.2a). Copper foil glued to the back of samples serves as a back gate. This sample design allows measurements and control of QHFm transition in ungated and gated regions separately and investigate transport across gate boundaries. We fabricated a number of samples with lithographical width of constrictions in the 1-15 μm range. The electrical width is reduced by $2 \cdot l_D = 200 - 400 \text{ nm}$ due to the depletion of a 2D electron gas near mesa edges caused by Ar ion milling, and by another $\approx 1.8l_D - 2.5\sqrt{a_B} \cdot l_D = 120 - 280 \text{ nm}$ (here Bohr radius $a_B = \hbar^2\epsilon/m_{eff}e^2$ is for CdTe dielectric constant $\epsilon = 10.3$ and effective electron mass $m_{eff} = 0.1m_e$) due to the formation of edge channels in the QHE regime [24], overall 0.5–1 μm reduction. Ohmic contacts are produced by soldering freshly cut indium pallets similar to previous studies [14, 16]. Electron transport is measured in a dilution refrigerator in a temperature range 30–650 mK with a standard ac technique using excitation current $\leq 1 \text{ nA}$.

RESULTS AND DISCUSSION

Ti front gate, evaporated directly on the CdTe surface, is found to modify surface pinning potential and reduce electron density under the gate by a factor of 2, see top panel in Fig. 2c. Sharp peaks near 3.5 T and 7 T are QHFm transitions due to Landau levels crossings modeled in Fig. 1a. Adjusting front and back gate voltages we can position the 7 T QHFm transition between $|1 \downarrow\rangle$ and $|0 \uparrow\rangle$ states within the $\nu = 2$, as shown in the middle and bottom panels in Fig. 2c. For the same electron densities in gated and ungated regions a slight difference in wavefunction profiles results in a difference in overlaps χ and in the field of QHFm transitions B^* . The difference $\Delta B^* = B^*_{ungated} - B^*_{gated}$ is in the 0–0.3 T range depending on cooldown parameters, on the wavelength of LED used, LED current and sample temperature during LED illumination. QHFm separation ΔB^* defines the gradient of Landau levels in the vicinity of a gate boundary, which controls the width of DWs [11, 12] and of the conducting channel formed along the gate boundary.

Magnetoconductance in the vicinity of the QHFm transition is plotted in Fig. 3, where $\nu = 2$ QHE state extends between 6.7 T < B < 8.2 T. $R_{xx} = 0$ below 7.0 T corresponds to a well-defined $\nu = 2$ state with $|1 \downarrow\rangle$ topmost energy state, while $R_{xx} = 0$ above 7.4 T is a $\nu = 2$ state with the topmost energy level $|0 \uparrow\rangle$. Resistance of the

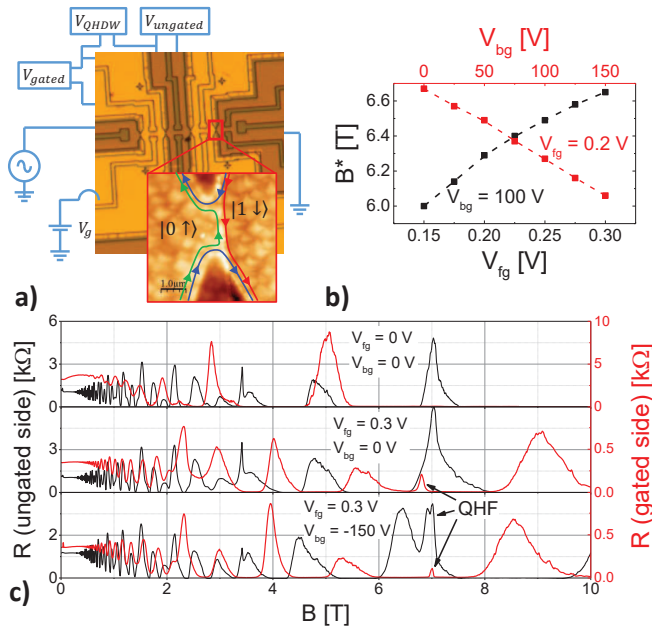


FIG. 2. (a) Photograph of one of the studied devices with measurement schematic. A bright orange is a metal gate. An AFM image of a constrictions with a gate boundary is shown in the inset. Blue, green and red lines represent $|0 \downarrow\rangle$, $|0 \uparrow\rangle$ and $|1 \downarrow\rangle$ chiral edge channels at $\nu = 2$. $|0 \uparrow\rangle$ and $|1 \downarrow\rangle$ channels hybridise forming a quantum Hall DW. (b) Dependence of QHFm position at filling factor $\nu = 2$ versus back gate (black dataset and black axis) and front gate (red dataset and red axis) voltages. (c) After cooldown densities under gate and outside the gate differs by a factor of 2-3 due to surface Fermi level pinning by gate. In order to align densities one need to apply high voltage on a front gate. After aligning densities and placing $\nu = 2$ in vicinity of QHFm transition one can observe QHFm transitions on both ungated and gated sides.

QHFm transition peak for wide regions shows activation behavior with an energy gap ≈ 1 K, see dashed lines in Fig. 3(b,c), the gap can be attributed to spin-orbit mixing of $|1 \downarrow\rangle$ and $|0 \uparrow\rangle$ states [22]. The center of QHFm transitions in gated region is at $B_{gated}^* = 7.14$ T, while for ungated $B_{ungated}^* = 7.25$ T. Transitions separation $\Delta B^* \approx 0.11$ T is large enough that resistance in the midpoint $B = 7.195$ T vanishes at low $T < 100$ mK. Thus, QHFm transition at a gate boundary should occur in the range $7.14 \text{ T} < B < 7.25 \text{ T}$. Indeed, as shown in the middle and the bottom panels in Fig. 3a resistance measured across gate boundaries peaks within that field range. For short channels $< 6 \mu\text{m}$ resistance saturates at low temperatures to a non-zero value, see Fig. 3(b,c) where temperature dependence of peak resistance for different channels in two different samples with $\Delta B^* = 0.11$ T for sample A and $\Delta B^* = 0.25$ T for sample B is plotted, with solid lines being fits to a constant + activation function. It is important to note that at $T < 100$ mK contribution of wide regions to R_{xx} is negligible, and peak resistance

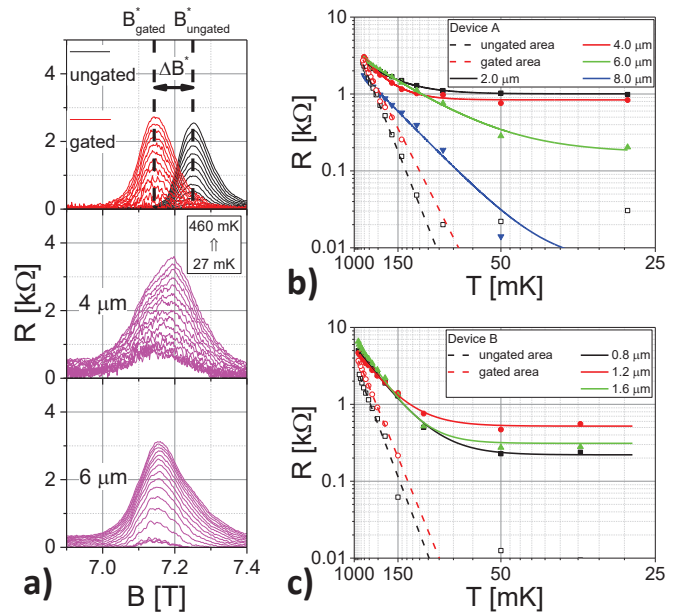


FIG. 3. (a) QHFm transitions for ungated and gated areas (black and red curves respectively; upper pane); resistance measured across 4 and 6 μm constrictions (middle and lower panes respectively). Dashed lines mark gated and ungated QHFm transitions which are separated by ΔB^* . Note that for the lowest temperature resistance across 6 μm constriction is almost vanishes, while resistance across 4 μm constriction saturates at low temperatures. (b,c) Temperature dependencies of resistances measured across constrictions of different widths in devices A and B. Dashed lines are for temperature dependencies of QHFm transitions in corresponding device.

reflects conduction through the channel formed along a gate boundary.

A hallmark of the electron transport through helical DWs is resistance invariance under magnetic field reversal because DWs are formed from two counter-propagating edges, Fig. 1b. Indeed, we found $R_{xx}(B) \approx R_{xx}(-B)$ for QHFm transitions measured across gate boundaries, Fig 4a. In contrast, presence of chiral edge states leads to $R_{xx}(B) \neq R_{xx}(-B)$, for example when $\nu = 1$ changes into $\nu = 2$ across the gate boundary $R_{xx}(-B) = 0$ while $R_{xx}(B) = 0.5e^2/h$, Fig 4b.

Now we analyze transport in short constriction at low temperatures, where saturation resistance is found to be < 2 k Ω in all measured samples. Here we refer to saturation resistances measured for B^* being close to the middle of the $\nu = 2$ plateaus in both gated and ungated regions; saturated resistance increases when B^* is shifted closer to the $\nu = 2$ boundary as shown in the supplementary material [25]. Within Landauer-Büttiker formalism resistance in the "ballistic" regime, where two non-interacting counter-propagating edge channels are formed along a gate boundary with no inter-channel scattering, is $0.5 h/e^2 = 12.9$ k Ω , Fig. 5. Parameterizing inter-channel

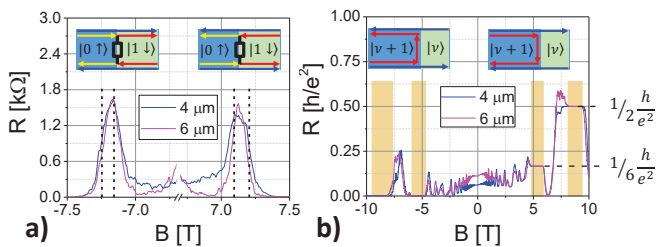


FIG. 4. (a) Resistances across different constriction formed between $|1 \downarrow\rangle$ and $|0 \uparrow\rangle$ states at $\nu = 2$ is the same for both field directions. Dashed lines mark position of ungated and gated QHFm peaks. (b) resistance across a chiral state formed between $\nu = 1$ and $\nu = 2$ states is quantized at $1/2 h/e^2$ and between $\nu = 2$ and $\nu = 3$ states at $1/6 h/e^2$ for positive field direction and is zero for negative fields.

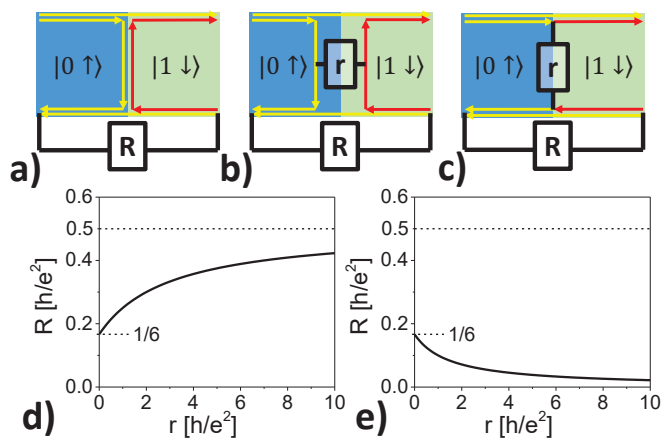


FIG. 5. Modeling of resistance R across a quantum Hall DW formed between $|1 \downarrow\rangle$ and $|0 \uparrow\rangle$ states. (a) In a ballistic regime there is no scattering between $|1 \downarrow\rangle$ and $|0 \uparrow\rangle$ channels and $R = 0.5 \frac{h}{e^2}$. In the presence of scattering parameterized by resistance r resistance R is plotted in (d) for model (b) and in (e) for model (c).

scattering by a resistor $0 < r < \infty$ reduces expected resistance down to $1/6 h/e^2 \approx 4.3 \text{ k}\Omega$, still much larger than measured values. Thus, the proper model for DWs is a single channel with backscattering, parameterized by effective channel resistance $r > 50 \text{ k}\Omega$ in Fig. 5c.

Transport in mesoscopic devices in the presence of disorder is characterized by conductance fluctuations [26]. Indeed, quasi-periodic conductance fluctuations are clearly observed in small channels, as shown in Fig. 6 for a $2 \mu\text{m}$ constrictions. Quasi-period ΔB of these oscillations is $\sim 40 - 55 \text{ mT}$. Similar quasi-periodic resistance fluctuations were observed in mesoscopic devices for transitions between neighboring quantum Hall states [27, 28]. One possible interpretation of resistance fluctuations is formation of a few domains with a small network of DWs spanning across the constriction. Some static

disorder, such as Mn doping fluctuations, potential fluctuations due to remote impurities, or surface roughness with characteristic size of $0.2 \mu\text{m}$ (see atomic force micrograph of the device surface in Fig. 6e), which result in the fluctuation of perpendicular component of magnetic field, may act as pinning centers for domain formation. Experimentally we found, though, that fluctuations pattern changes drastically every time magnetic field is ramped outside the $\nu = 2$ state, Fig. 6b, which means that dynamic fluctuations rather than static impurities define the conduction path within the channel. We also note that the width of the gate-defined potential gradient, which defines the width of the conductive channel, is of the order of the 2D gas-to-gate distance 100 nm , of the same order as the width of a DWs [11], which makes formation of multiple domains within the channel quite unlikely. Assuming the width of the conduction path to be 100 nm , period of quasi-periodic oscillations translates into $0.1 \times 0.8 - 1.1 \mu\text{m}$ elongated area which spans most of the estimated electrical width of the $2 \mu\text{m}$ constriction. From exponential decay of fluctuation's amplitude we estimate the phase coherence length $l_\phi \propto T^{-1} = 1 - 2 \mu\text{m}$ at the base temperature, see Supplementary materials [25].

Theoretically, transport in the QHFm regime should differ markedly from the transport carried by edge states along sample boundary. At sample boundary low lying Landau levels always cross Fermi energy forming conducting channels. At a QHFm transition significant Rashba spin-orbit interaction results in $\Delta_R \approx 50 \mu\text{eV}$ anticrossing gap between $|0 \uparrow\rangle$ and $|1 \downarrow\rangle$ levels which form DWs [22]. Thus, there should be no conduction in the QHFm transition regime at low temperatures, consistent with vanishing resistance in wide samples. However, disorder results in the broadening of Landau levels and introduces extended states within the spin-orbit gap, as illustrated in Fig. 6d. The Δ_R gap is smaller than the cyclotron gap $0.1 - 0.3 \text{ T}$ away from the transition ($\hbar\omega_c = 1.09 \text{ meV/T}$, or $50-150 \mu\text{eV}$) and in-gap states are extended enough to hybridize and provide a conduction path at low temperatures. These in-gap states seems to be primarily defined by weakly localized charges in the tails of the Landau levels since large B change alters the interference pattern, also pattern slowly changes over several hours even if the field is kept close to the QHFm transition.

In order to calculate transport through such channels of in-gap states we model a single QHFm DW numerically, see Supplemental material for details [25]. In the model we assume that the primary source of localized states are potential fluctuations due to remote doping and used zero-field mobility to calculate the strength and the density of the fluctuations. In the model we also include surface roughness, which leads to the deviation of magnetic field orientation and orientation of Mn spins from the z -direction at high fields, effec-

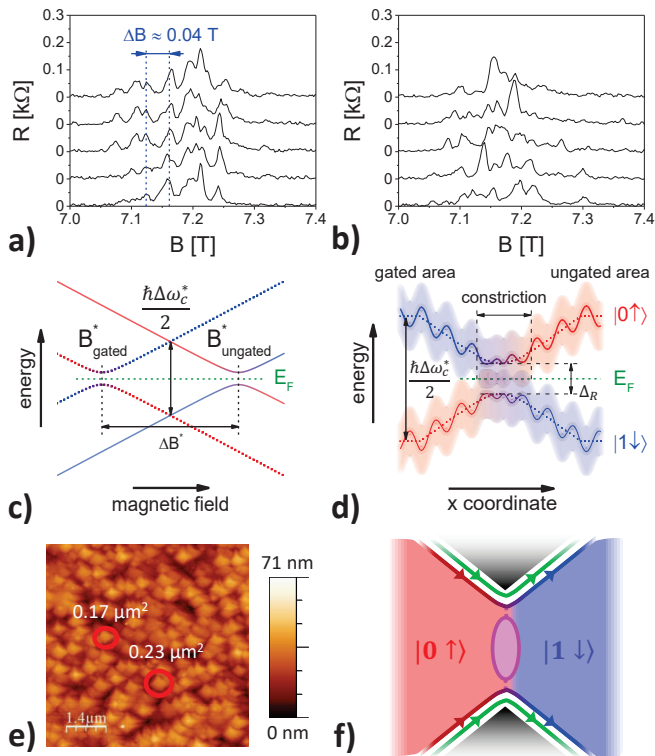


FIG. 6. (a) Fluctuations of resistance across a $2 \mu\text{m}$ constriction measured at a base temperature $T = 27 \text{ mK}$ while magnetic field was swept in a narrow range 6.8-7.5 T. Fluctuations have similar pattern with a quasi-period of $\Delta B \sim 40 \text{ mT}$. (b) Fluctuation pattern changes drastically after wide B sweeps 5-10 T. (c) Energy levels in the vicinity of the QHFm transition for gated (dotted lines) and ungated (solid lines) regions. (d) Energy diagram of a DW formed at the gate boundary, wiggling lines indicate schematically a role of disorder and shaded areas are localized states in the tails of Landau levels. Conduction occurs via extended localized states in the middle of the gap, creating a conductive channel of helical nature. (e) Atomic force microscopy image of the wafer surface morphology. (f) Schematic of a conducting channel which provides backscattering between $\nu = 2$ edge states. Magenta path forms a loop responsible for the interference pattern which leads to the resistance fluctuations.

tively a magnetic disorder. Thus calculated conductivity of a DW dominated by the conduction via in-gap states is $0.146 \pm 0.026 \frac{e^2}{h}$, which is in good agreement with the measured resistance across the constriction $R = 0.66 - 0.87 \text{ k}\Omega$ if we use the model in Fig.5c to convert the channel conductance into measured resistance. Most importantly, theoretical modeling shows that wavefunctions of the in-gap states retain the helical character of the DWs, similarly to the helical properties of spin-orbit states in quantum dots [29]. Such feature provides a necessary ingredient for the formation of a spinless p-wave superconducting order in the presence of s-wave superconducting proximity effect.

SUMMARY

In this work we demonstrated gate control of QHFm transition at $\nu = 2$ in high mobility 2D gases in CdTe:Mn heterostructures and investigated conducting channels formed along domain walls at the boundary between ferromagnetic domains. We show that for long channels conduction is suppressed at low temperatures, consistent with spin-orbit-induced anticrossing of Landau levels, but for short ($< 4 \mu\text{m}$) channels conduction saturates at low temperatures. Conduction through these channels does not depend on the direction of magnetic field, unlike conduction through chiral channels formed at the boundary of different QHE states. We expect that the in-gap states, which dominate the conduction, retain the helical character of domain walls and, thus, should have large overlap with s-wave superconductors forming a building block for an electrostatically reconfigurable network of topological superconductors.

ACKNOWLEDGMENTS

Authors acknowledge support by the Department of Defense Office of Naval research Award N000141410339 (A.K, T.W., G.S., Y. L-G. and L.R.) and by the National Science Centre (Poland) grant DEC-2012/06/A/ST3/00247 (V.K., Z.A., G.K., and T.W.) and by the Foundation for Polish Science through the IRA Programme financed by EU within SG OP Programme (V.K., Z.A., G.K., and T.W.).

* leonid@purdue.edu

- [1] A. Kitaev, *Physics-Uspekhi* **44**, 131 (2001).
- [2] C. Nayak, A. Stern, M. Freedman, and S. Das Sarma, *Reviews of Modern Physics* **80**, 1083 (2008).
- [3] R. M. Lutchyn, J. D. Sau, and S. Das Sarma, *Physical Review Letters* **105**, 077001 (2010).
- [4] Y. Oreg, G. Refael, and F. von Oppen, *Physical Review Letters* **105**, 177002 (2010).
- [5] L. P. Rokhinson, X. Liu, and J. K. Furdyna, *Nature Physics* **8**, 795 (2012).
- [6] V. Mourik, K. Zuo, S. Frolov, S. Plissard, E. Bakkers, and L. Kouwenhoven, *Science* **336**, 1003 (2012).
- [7] A. Das, Y. Ronen, Y. Most, Y. Oreg, M. Heiblum, and H. Shtrikman, *Nature Physics* **8**, 887 (2012).
- [8] S. M. Albrecht, A. P. Higginbotham, M. Madsen, F. Kuemmeth, T. S. Jespersen, J. Nygård, P. Krogstrup, and C. M. Marcus, *Nature* **531**, 206 (2016).
- [9] M. T. Deng, S. Vaitiekenas, E. B. Hansen, J. Danon, M. Leijnse, K. Flensberg, J. Nygard, P. Krogstrup, and C. M. Marcus, *Science* **354**, 1557 (2016).
- [10] J. Wiedenmann, E. Bocquillon, R. S. Deacon, S. Hartinger, O. Herrmann, T. M. Klapwijk, L. Maier, C. Ames, C. Brne, C. Gould, A. Oiwa, K. Ishibashi,

- S. Tarucha, H. Buhmann, and L. W. Molenkamp, *Nature Communications* **7**, 10303 (2016).
- [11] V. I. Fal'ko and S. Iordanskii, *Physical Review Letters* **82**, 402 (1999).
- [12] V. I. Fal'ko and S. V. Iordanskii, *Physical Review Letters* **84**, 127 (2000).
- [13] E. De Poortere, E. Tutuc, J. Papadakis, and M. Shayegan, *Science* **290**, 1546 (2000).
- [14] J. Jaroszyński, T. Andrearczyk, G. Karczewski, J. Wróbel, T. Wojtowicz, E. Papis, E. Kamińska, A. Piotrowska, D. Popović, and T. Dietl, *Physical Review Letters* **89**, 266802 (2002).
- [15] J. Eisenstein, H. Stormer, L. Pfeiffer, and K. West, *Physical Review B* **41**, 7910 (1990).
- [16] C. Betthausen, P. Giudici, A. Iankilevitch, C. Preis, V. Kolkovsky, M. Wiater, G. Karczewski, B. A. Piot, J. Kunc, M. Potemski, T. Wojtowicz, and D. Weiss, *Physical Review B* **90**, 115302 (2014).
- [17] B. E. Feldman, A. J. Levin, B. Krauss, D. A. Abanin, B. I. Halperin, J. H. Smet, and A. Yacoby, *Physical Review Letters* **111**, 076802 (2013).
- [18] D. J. Clarke, J. Alicea, and K. Shtengel, *Nature Communications* **4**, 1348 (2013).
- [19] R. S. K. Mong, D. J. Clarke, J. Alicea, N. H. Lindner, P. Fendley, C. Nayak, Y. Oreg, A. Stern, E. Berg, K. Shtengel, and M. P. A. Fisher, *Physical Review X* **4**, 011036 (2014).
- [20] B. Verdene, J. Martin, G. Gamez, J. Smet, K. von Klitzing, D. Mahalu, D. Schuh, G. Abstreiter, and A. Yacoby, *Nature Physics* **3**, 392 (2007).
- [21] T. Wojtowicz, M. Kutrowski, G. Karczewski, J. Kossut, B. König, A. Keller, D. Yakovlev, A. Waag, J. Geurts, W. Ossau, G. Landwehr, I. Merkulov, F. Teran, and M. Potemski, *Journal of Crystal Growth* **214-215**, 378 (2000).
- [22] A. Kazakov, G. Simion, Y. Lyanda-Geller, V. Kolkovsky, Z. Adamus, G. Karczewski, T. Wojtowicz, and L. P. Rokhinson, *Physical Review B* **94**, 075309 (2016).
- [23] F. Teran, M. Potemski, D. Maude, T. Andrearczyk, J. Jaroszyński, T. Wojtowicz, and G. Karczewski, *Physical Review B* **82**, 245120 (2010).
- [24] D. B. Chklovskii, B. I. Shklovskii, and L. I. Glazman, *Physical Review B* **46**, 4026 (1992).
- [25] See Supplemental Material at [URL will be inserted by publisher] for [give brief description of material],.
- [26] P. A. Lee, A. D. Stone, and H. Fukuyama, *Physical Review B* **35**, 1039 (1987).
- [27] J. K. Jain and S. A. Kivelson, *Physical Review Letters* **60**, 1542 (1988).
- [28] J. A. Simmons, S. W. Hwang, D. C. Tsui, H. P. Wei, L. W. Engel, and M. Shayegan, *Physical Review B* **44**, 12933 (1991).
- [29] I. Aleiner and V. Fal'ko, *Physical Review Letters* **87** (2001), 10.1103/physrevlett.87.256801.

Supplementary Materials

MESOSCOPIC TRANSPORT IN ELECTROSTATICALLY-DEFINED SPIN-FULL CHANNELS IN QUANTUM HALL FERROMAGNETS

AFM IMAGES OF SAMPLES

Images of constrictions with the gate boundaries are shown in Fig. S1. Numbers indicate lithographical width of constrictions along gate boundaries.

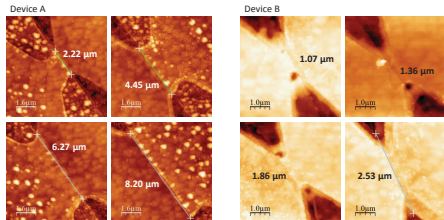


FIG. S1. AFM micrographs of Devices A and B. A faint line across the constriction is the Ti gate boundary.

2DEG PREPARATION

We found that condition of LED illumination has a great impact on the width and electrostatic control of the QHFm transition. Illumination of a sample with red LED at ~ 10 K results in very wide (0.5 – 0.8 T) QHFm transition which position is sensitive to the gate voltage (0.3 – 0.4 T per 100 V on a back gate voltage). Similar results were obtained by illuminating sample with a green LED at low temperatures ~ 200 mK. Illumination with green LED at high temperatures (~ 10 K) results in a 2D gas with $\sim 30\%$ higher carrier density and narrow (0.1 – 0.3 T) QHFm transition which position is almost insensitive to the applied gate voltage.

The optimal QHFm transition width and control was achieved by illuminating samples with green LED at low temperatures and subsequent heating to 1 K, where after 2-4 hours 2D gas the system relaxed into an intermediate state with 0.2 – 0.4 T - wide QHFm transition and 0.1 – 0.2 T/100 V transition control. Thus prepared 2D gases vary slightly between cooldowns for the same sample and between different samples.

LOCAL HEATING BY EXCITATION CURRENT.

Dependence of resistance across gate boundaries for different constriction sizes measured at base $T < 30$ mK is shown in Fig.S2. We conclude that for excitation currents $I_{ac} < 1$ nA Joule heating is negligible.

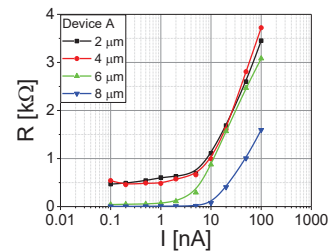


FIG. S2. Dependence of resistance across gate boundaries for different channel lengths on excitation current at a base temperature $T = 27$ mK.

DEPENDENCE OF CONDUCTANCE FLUCTUATIONS ON ΔB^* .

Separation of QHFm transitions in gated and ungated regions ΔB^* reflects the value of the s-d exchange gradient near the gate boundary and, as a result, position of ferromagnetic domains formation. For $\Delta B^* = 0$ there is no s-d exchange gradient and domains are randomly formed within the 2D plane. Narrow field sweeps within $7.3 T < B < 7.5 T$ range across the QHFm transition results in the formation of different domain configurations, different conduction paths and different patterns of conduction fluctuations, Fig. S3(a). Often there is no domain wall formed in the vicinity of the constriction, in this case no conduction is observed as shown for the up-sweep in (a). In contrast, for $\Delta B^* = 0.2$ T the gate-induced s-d exchange gradient stabilizes the domain wall position and conducting channels are always formed. The conduction channel is well defined and the resistance fluctuations pattern is reproducible over multiple field sweeps, Fig. S3(b).

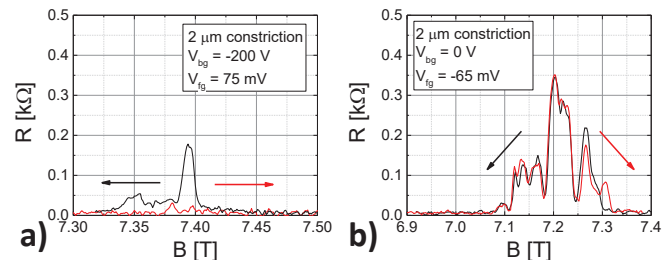


FIG. S3. Mesoscopic resistance fluctuations for 2 μ m channels are shown for (a) $\Delta B^* = 0$ and (b) $\Delta B^* = 0.2$ T. For each temperature point consecutive B -scans in both field directions were recorded.

TIME EVOLUTION OF MESOSCOPIC FLUCTUATIONS.

Even for large QHfM transitions separation $\Delta B^* = 0.2$ T and at the lowest $T < 30$ mK there is a slow change in the pattern of resistance fluctuations with time, Fig. S4. A characteristic time scale for the pattern change is ~ 7 hours, as determined from a half width at the half height of the autocorrelation function $F(\Delta t) = \langle R(t)R(t + \Delta t) \rangle$. Most likely the conduction path and the fluctuation pattern are affected by gate voltage-induced slow motion of localized charges in the vicinity of the conduction channel.

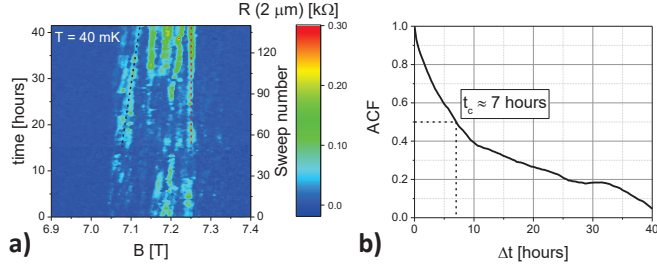


FIG. S4. Time evolution of resistance fluctuations in a $2 \mu\text{m}$ channel is plotted in the color plot for $\Delta B^* = 0.2$ T and $T = 40$ mK. Data was recorded for $B = 6.9$ T \rightarrow 7.4 T sweeps. (b) resistance auto-correlation function as a function of time offset Δt .

DEPENDENCE OF HELICAL CHANNEL CONDUCTANCE ON THE POSITION OF B^* WITHIN THE $\nu = 2$ PLATEAU.

The value of maximum resistance of the conducting channel formed between states with opposite polarization depends not only on the length of the channel and QHfM separation ΔB^* , but also on the position of the QHfM transition within the $\nu = 2$ plateau. In Fig. S5 we simultaneously change density in gated and ungated regions and sweep QHfM in the channel $\langle B^* \rangle = (B_{\text{gated}}^* + B_{\text{ungated}}^*)/2$ across the $\nu = 2$ plateau while keeping ΔB^* approximately constant. Magnetoresistance in the gated and ungated regions is plotted in the left plot, and across the $2 \mu\text{m}$ constriction in the right plot. In the inset resistance saturation value R_0 and activation energy E_a are extracted from temperature dependence of peak resistance. It is clear that extrema of R_0 and E_a depend on the position of $\langle B^* \rangle$ within the $\nu = 2$ plateau, with minimum R_0 and maximum E_a occur at $\nu = 2$. Data in the main text is taken for $\langle B^* \rangle$ placed close to the center of the $\nu = 2$ plateau in both gated and ungated regions.

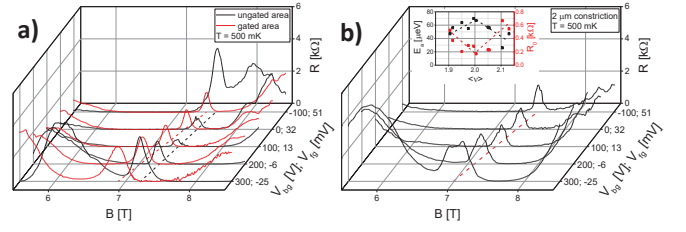


FIG. S5. R_{xx} in the vicinity of $\nu = 2$ QHE state is plotted for gated and ungated regions (left) and across a $2 \mu\text{m}$ constriction for different front gate V_{fg} and back gate V_{bg} voltages at $T = 500$ mK. Here position of the QHfM transition $\langle B^* \rangle$ is shifting relative to the center of the $\nu = 2$ plateau in both gated and ungated regions. In the inset the value of saturation resistance R_0 and activation energy E_a are plotted as a function of a filling factor $\langle B^* \rangle$, where R_0 and E_a are extracted from fits of temperature dependence of peak value of the resistance to a constant + activation function.

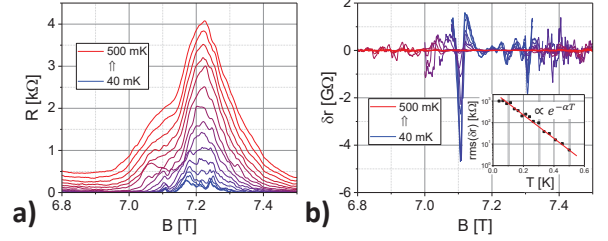


FIG. S6. (a) Resistance R across $2 \mu\text{m}$ constriction at different temperatures. (b) Corresponding fluctuations δr of resistance r along gate boundary. Inset shows standard deviation of resistance across $2 \mu\text{m}$ constriction.

TEMPERATURE DEPENDENCE OF RESISTANCE FLUCTUATIONS AND PHASE COHERENCE LENGTH

Temperature dependence of resistance fluctuations across a $2 \mu\text{m}$ constriction is shown in Fig. S6a, where magnetic field was swept in a narrow range near the the QHfM transition (6.8-7.5 T) in order to preserve the fluctuation pattern. Channel resistance r can be calculated from the measured resistance R using Landauer-Büttiker formalism discussed in the main text:

$$r = \frac{1 - 6R}{4R}, \quad (\text{S1})$$

where both r and R are expressed in units of h/e^2 . Fluctuations of the measured resistance δR are obtained by subtracting a smooth background from the resistance R , and fluctuations of the resistance of the conducting channel δr are calculated as

$$\delta r = \frac{dr}{dR} \delta R = -\frac{1}{4} \frac{\delta R}{R^2}. \quad (\text{S2})$$

Thus extracted fluctuations of channel resistance are plotted in Fig. S6b for a wide temperature range. In the

inset rms amplitude of δr is plotted as a function of temperature. From exponential decay of rms(δr) with temperature $rms \propto e^{-T_0/T} = e^{-L/l_\phi(T)}$, $T_0 = 80\text{mK}$, we estimate that phase coherence length l_ϕ exceeds $\approx 800\text{ nm}$ below 100 mK for $L \approx 1\ \mu\text{m}$. Thus the phase coherence is preserved over the length of the channel.

MODELING OF DOMAIN WALL CONDUCTION IN THE QHFM REGIME.

In order to model our system, we consider N electrons confined to a $L_x \times L_y$ rectangle, subjected to magnetic field $B = -B\hat{e}_z$. We take $N = [\nu L_x L_y / 2\pi\ell^2]$, where ℓ is the magnetic length and $\nu = 2$ is the filling factor.

$$H_s = \sum_i \left[\frac{1}{2m^*} \left(\mathbf{p}_i + \frac{e\mathbf{A}}{c} \right)^2 + \frac{\beta_R}{\hbar} \left(\mathbf{p}_i \frac{e\mathbf{A}}{c} \right) \times \boldsymbol{\sigma}_i + V_G(\mathbf{r})\sigma_{z,i} + V_{\text{imp}}(\mathbf{r}) + V_{\text{fl}}^{\text{mag}}(\mathbf{r})\sigma_z \right] + \frac{e^2}{2\epsilon_r} \sum_{i,j} \frac{1}{|\mathbf{r}_i - \mathbf{r}_j|} \quad (\text{S3})$$

Here $m^* = 0.1m$ is the effective electron mass in CdTe and β is the Rashba constant. The spin dependent potential V_G mimics variation of Zeeman energy across the sample as a result of applied gate voltage. We consider remote impurity potential $V_{\text{imp}}(\mathbf{r}) = \sum_i^{N_i} w_i \exp[-(\mathbf{r} - \mathbf{r}_i)^2/d^2]$, where the number of impurities $N_i = N$ and r_i 's denote the position of the randomly placed impurities in the doping layer and $w_i \in [-W, W]$. Surface roughness (see Fig. 6e of the main text) translates into curvy profile of the quantum well, and as a consequence, into the deviation of magnetic field orientation hence Mn spin orientation from z-direction. In order to model this effect of surface roughness we introduce the spin dependent random potential $V_{\text{fl}}^{\text{mag}}(\mathbf{r}) = \sum_i u_i \exp[-(\mathbf{r} - \mathbf{r}_i)^2/b^2]\sigma_z$. We choose $W = 8\text{ meV}$, $d = 40\text{ nm}$, and $u = 15\ \mu\text{eV}$ and $b = 150\text{ nm}$. Parameters for remote dopants are chosen to be consistent with the electron mobility that has been measured experimentally ($\mu = 30,000\text{ cm/Vs}$ at $B = 0$). The electron-electron interaction is taken into

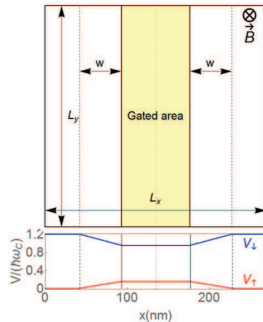


FIG. S7. Schematic view of the simulated system and the spin dependent potential due to gate voltage

account using the Hartree-Fock approximation. The self-consistent procedure is done in the basis set of five orbital Landau states, each with two spin projections. In our numerical procedure, the spin-dependent potential and random impurities are chosen to be symmetric with respect to the reflection about a line parallel to the y -axis that bisects L_x ; $V_G(x, y) = V_G(L_x - x, y)$ and $x_{N/2+i} = L/2 - x_i$, $y_{N/2+i} = y_i$. Periodic boundary conditions are used in both x and y directions. The Hartree-Fock procedure reduces the Hamiltonian to a non-diagonal and non-local effective single particle form [1].

We compute the conductance of our finite system using Green's function approach [2]. Knowing the single particle Hartree-Fock and impurity potential, we discretize the problem on a lattice of $N_x \times N_y$ points. We place our leads in the channels separated by $L_y/2$. The Hamiltonian describing the system with leads is given by

$$H_t = H_s + H_1 + H_2 + V_{1s} + V_{2s}, \quad (\text{S4})$$

where H_i describes the lead, V_{is} the coupling between lead and the localized electron states in the domain wall area ($i = 1, 2$ label the lead). The conductance is given by

$$G = \frac{e^2}{h} \text{Tr} \left(\hat{\Gamma}_1 \hat{\mathcal{G}}_R \hat{\Gamma}_2 \hat{\mathcal{G}}_A \right), \quad (\text{S5})$$

where $\mathcal{G}_{R/A}$ denotes the retarded (advanced) Green's function of the interacting electron gas, $\hat{\mathcal{G}}_{A,R} = [(E \pm i\eta)\hat{I} - \hat{H}]^{-1}$, E is the energy (we take $E = E_F$), $\hat{\Gamma}_i = i(\hat{\Sigma}_i^R - \hat{\Sigma}_i^A)$ are the coupling matrices, and the contact retarded and advanced self-energies $\hat{\Sigma}_i^R$ and $\hat{\Sigma}_i^A$ are given by

$$\hat{\Sigma}_i^R = V_{is}^\dagger \left[(E + i\eta)\hat{I} - \hat{H}_i \right]^{-1} \hat{V}_{is} \quad (\text{S6})$$

$$\hat{\Sigma}_i^A = V_{is}^\dagger \left[(E - i\eta)\hat{I} - \hat{H}_i \right]^{-1} \hat{V}_{is}. \quad (\text{S7})$$

We compute conductance using (S5) and extract conductivity of the DW σ_{yy} . When both magnetic and remote impurities are present, the averaged conductivity for five realizations of disorder is found to be $\sigma_{yy} = 0.146 \pm 0.023 \frac{e^2}{h}$. If magnetic fluctuations are ignored, we obtain $\sigma_{yy} = 0.105 \pm 0.018 \frac{e^2}{h}$. The calculated value $\sigma_{yy} = 0.146 \frac{e^2}{h}$ corresponds to the channel resistance $r = 1/\sigma_{yy} = 177\text{ k}\Omega$ or $R = 0.77\text{ k}\Omega$. This value of R is in a good agreement with the measured resistance $R \approx 0.5 - 0.7\text{ k}\Omega$, suggesting that the model captures the essential physics of conduction in the channels formed along domain walls.

* leonid@purdue.edu

- [1] Giuliani G. and Vignale G., *Quantum Theory of the Electron Liquid* (Cambridge University Press, 2005).
- [2] Ferry D.K., Goodnick S.M., and Bird J., *Transport in Nanostructures* (Cambridge University Press, 2009).